Exp Fluids (2016) 57:61
DOI 10.1007/s00348-016-2141-9

RESEARCH ARTICLE

The effect of ambient pressure on ejecta sheets from free-surface ablation

J. O. Marston[1] · M. M. Mansoor[2] · S. T. Thoroddsen[2] · T. T. Truscott[3]

Received: 13 December 2015 / Revised: 30 January 2016 / Accepted: 7 February 2016 / Published online: 16 April 2016

Abstract We present observations from an experimental study of the ablation of a free liquid surface promoted by a focused laser pulse, causing a rapid discharge of liquid in the form of a very thin conical-shaped sheet. In order to capture the dynamics, we employ a state-of-the-art ultra-high-speed video camera capable of capturing events at 5×10^6 fps with shutter speeds down to 20 ns, whereby we were able to capture not only the ejecta sheet, but also the shock wave, emerging at speeds of up to 1.75 km/s, which is thus found to be hypersonic (Mach 5). Experiments were performed at a range of ambient pressures in order to study the effect of air drag on the evolution of the sheet, which was always observed to dome over, even at pressures as low as 3.8 kPa. At reduced pressures, the extended sheet evolution led to the formation of interference fringe patterns from which, by comparison with the opening speed of rupture, we were able to determine the ejecta thickness.

Electronic supplementary material The online version of this article (doi:10.1007/s00348-016-2141-9) contains supplementary material, which is available to authorized users.

✉ J. O. Marston
jeremy.marston@ttu.edu

[1] Department of Chemical Engineering, Texas Tech University, Lubbock, TX 79409, USA

[2] Division of Physical Sciences and Engineering, King Abdullah University of Science and Technology, Thuwal 23955-6900, Saudi Arabia

[3] Department of Mechanical and Aerospace Engineering, Utah State University, Logan, UT 84322, USA

1 Introduction

The formation and dynamics of ejecta sheets and jets is a fundamentally significant area in fluid dynamics. The aerosols and sprays resulting from their fragmentation can become extremely small and suspended in air (Villermaux 2007; Bird et al. 2010). Recently, it has been shown both numerically (e.g., Thoraval et al. 2012) and experimentally (e.g., Thoroddsen et al. 2011) that ejecta sheets from droplet impact can reach submicron thicknesses, therefore implying that droplets produced via fragmentation of these sheets will also be submicron (Lhuissier and Villermaux 2012)

The explosive discharge of matter, and in particular fine droplets, following a laser pulse has been reported in a variety of investigations: Explosive droplet vaporization was reported by Kafalas and Herrmann (1973), Armstrong (1984), Chitanvis (1986), Eickmans et al. (1987), Hsieh et al. (1987), Carls and Brock (1988) and Lindinger et al. (2004) for freely falling droplets; Apitz and Vogel (2005) studied the ejection of material during the ablation of soft tissues as well as water when a laser pulse was focused near the free surface; Thoroddsen et al. (2009) and Heijnen et al. (2009) reported the generation of jets and sprays from a laser pulse focused into a sessile droplet with speeds up to 1.4 km/s; Tagawa et al. (2012) used small capillary tubes to create slender jets with speeds up to 850 m/s; Marston and Thoroddsen (2015) created the simultaneous release of multiple micro-jets by focusing a laser into the interior of a particle-coated droplet.

Here, we explore the ablation of a flat free surface (most recently reported by Chen et al. 2013 and Zhiyuan et al. 2014) at reduced ambient pressure with the aid of a novel ultra-high-speed video camera. An example of the ablation dynamics is presented in Fig. 1, which scholars familiar

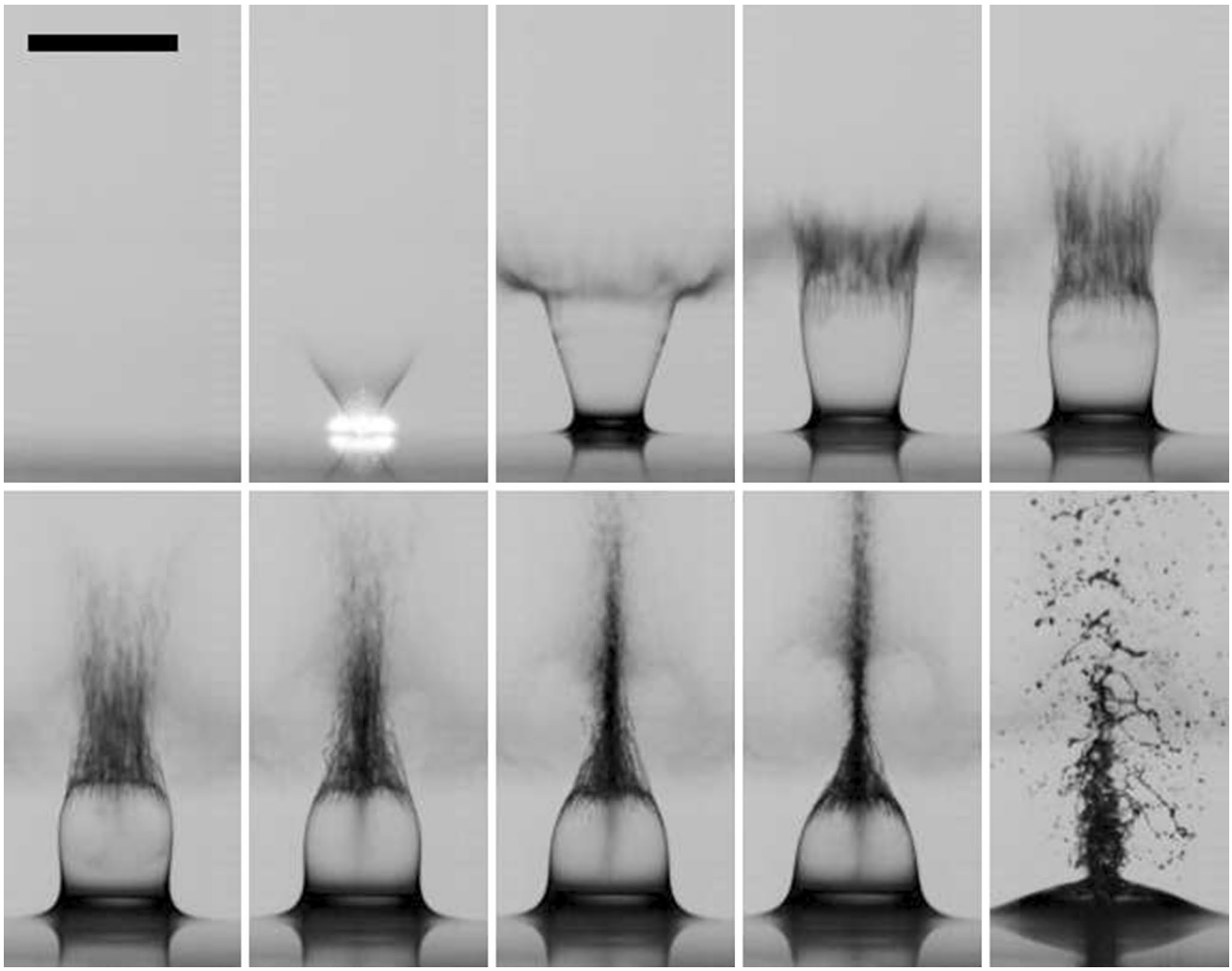

Fig. 1 Example sequence showing the result of a laser pulse focused at the free surface under atmospheric pressure, $P \approx 101$ kPa. The bright spot in frame 2 is the residual plasma. Images are taken at times $t = -2.9$, 2.9, 8.8, 14.7, 20.6, 26.4, 32.3, 38.2, 44.1 and 162 μs from the laser pulse. The *scale bar* is 2 mm

with water entry will recognize as being qualitative similar in appearance to the splash sheet resulting from sphere impact onto quiescent water pools; note that this phenomena also exhibit a buckling-type instability, reported by Marston et al. (2015). In this study, we pay special attention to the ejecta sheet and its corresponding thickness as part of the ablation dynamics.

2 Experimental

A schematic of the experiment is shown in Fig. 2. A 7-ns laser pulse (Quantel Ultra 50, 532 nm) is focused through a microscope objective to the free surface of a small liquid pool (25 mm in diameter, 10 mm deep). The pool itself is housed in a small custom-built vacuum chamber (TSE Troller AG, Switzerland) in order to vary the ambient

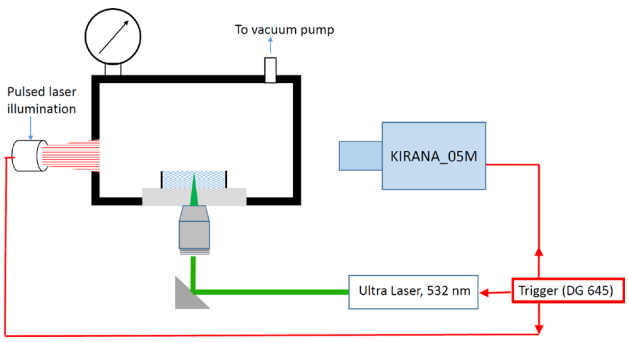

Fig. 2 Schematic representation of the experimental setup

pressure. To capture the rapid motions in these experiments, we employ a state-of-the-art high-speed video camera (Kirana-05M, Specialised Imaging, UK) which can

record 180 frames continuously at rates of up to 5 million fps with a fixed pixel resolution of 924 × 768 using an in situ storage sensor. For back-lighting, we synchronized the camera with a pulsed laser illumination system emitting 20 ns pulses at 640 nm. Thus, although the minimum shutter speed used was 100 ns, the effective exposure time is set by the pulsed illumination time. The laser pulse, camera and illumination were all triggered using a delay generator (Stanford Research Systems, DG645). In addition, we used a Phantom V1610 high-speed camera to record longer duration video clips than with the Kirana-05M, due to its limit of 180 frames.

The focal waist of the laser beam could not be measured directly due to the extremely bright emission from the plasma formation. However, given that the effective focal length of the lens is 20 mm and that the beam divergence is 2.5 mrad, the optical invariant dictates that the spot size is approximately 50 μm. Thus, given the repeatability of the experiment, we can assume a maximum uncertainty in spatial location of the focal spot of 50 μm.

Fig. 3 Example sequence showing the result of a laser pulse focused a few millimeters below the surface. The *arrows* in frames 2, 3 and 4 indicate the growth and collapse of the cavitation bubble, responsible for the crown formation. Images are taken at times $t = -10$, 52, 114, 177, 239, 302, 427, 552 and 1052 μs from the laser pulse. The *scale bar* is 2 mm. The cavitation bubble appears off-axis with the jet due to refraction

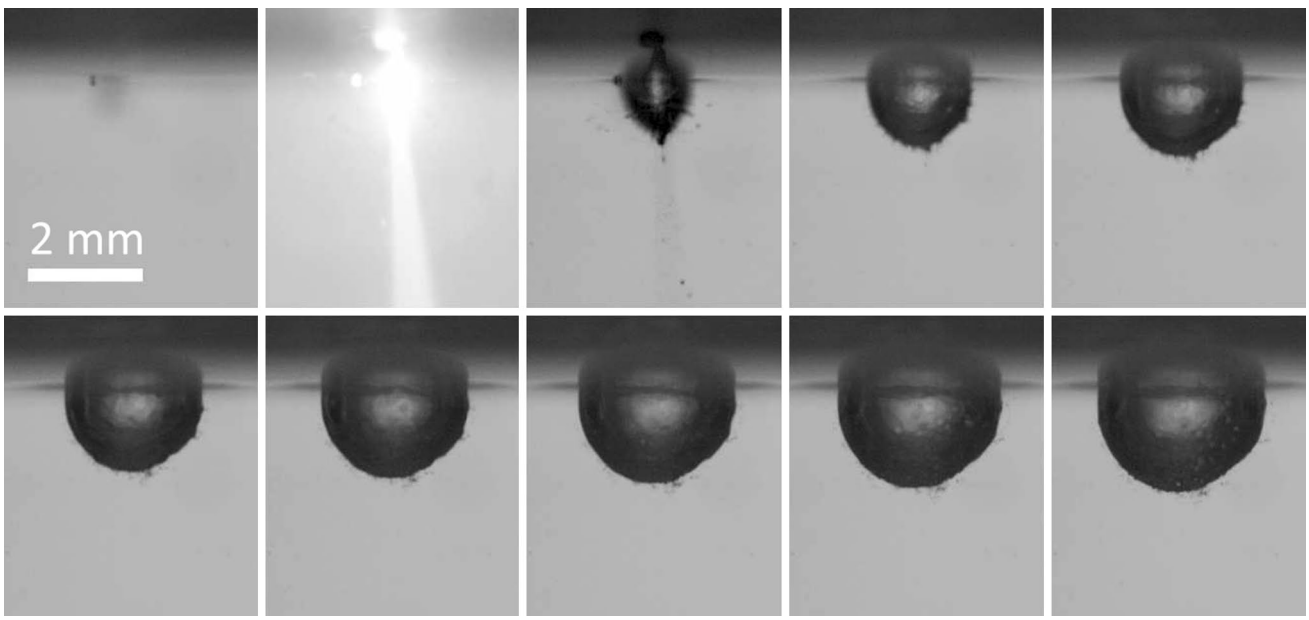

Fig. 4 Example sequence showing the cavitation bubble growth below the surface. The laser pulse is clearly identified in image 2 of the sequence by the bright emission. Images are taken at times $t = -13$, 0, 13, 39, 65, 92, 118, 144, 171 and 197 μs from the laser pulse. The *scale bar* is 2 mm

3 Results and discussion

The location of the laser focal point relative to the free surface is a key variable in determining the repeatability of the ablation process. As such, great care was taken to ensure the laser was focused precisely at the free surface by maintaining a constant water level and using a micrometer to adjust the position of microscope lens below the vacuum chamber. To highlight the dramatic difference in the dynamics by changing the focal point, Fig. 3 shows an image sequence from a video taken for a laser pulse focused just below the free surface. Here, we observe the emergence of a slender jet, followed by a crown-like formation, which is qualitatively similar to the observations of Chen et al. (2013) for laser-induced cavitation below a flat free surface and Heijnen et al. (2009) for liquid droplets. Below the surface, we observe the initial growth and collapse of the bubble and further oscillations. It is the re-expansion of the bubble below the surface which gives rise to the crown formation following the jet. In this realization, the initial jet speed is $V_{\text{jet}} = 18.8$ m/s.

The effect of varying the laser focal depth relative to the free surface was discussed in the context of both drops (Thoroddsen et al. 2009) and flat free surfaces (Chen et al. 2013), and since the primary focus of this study was the effect of ambient air pressure, we restrict our attention hereafter to trials where the laser focal point was at the free surface, such as that shown in Fig. 1; this sequence exhibits the rapidity of the phenomenon, with the expansion and closure of the crown formation taking place within 30 μs from the laser pulse. Given the associated length scale of this process, which one could take as the crown diameter,

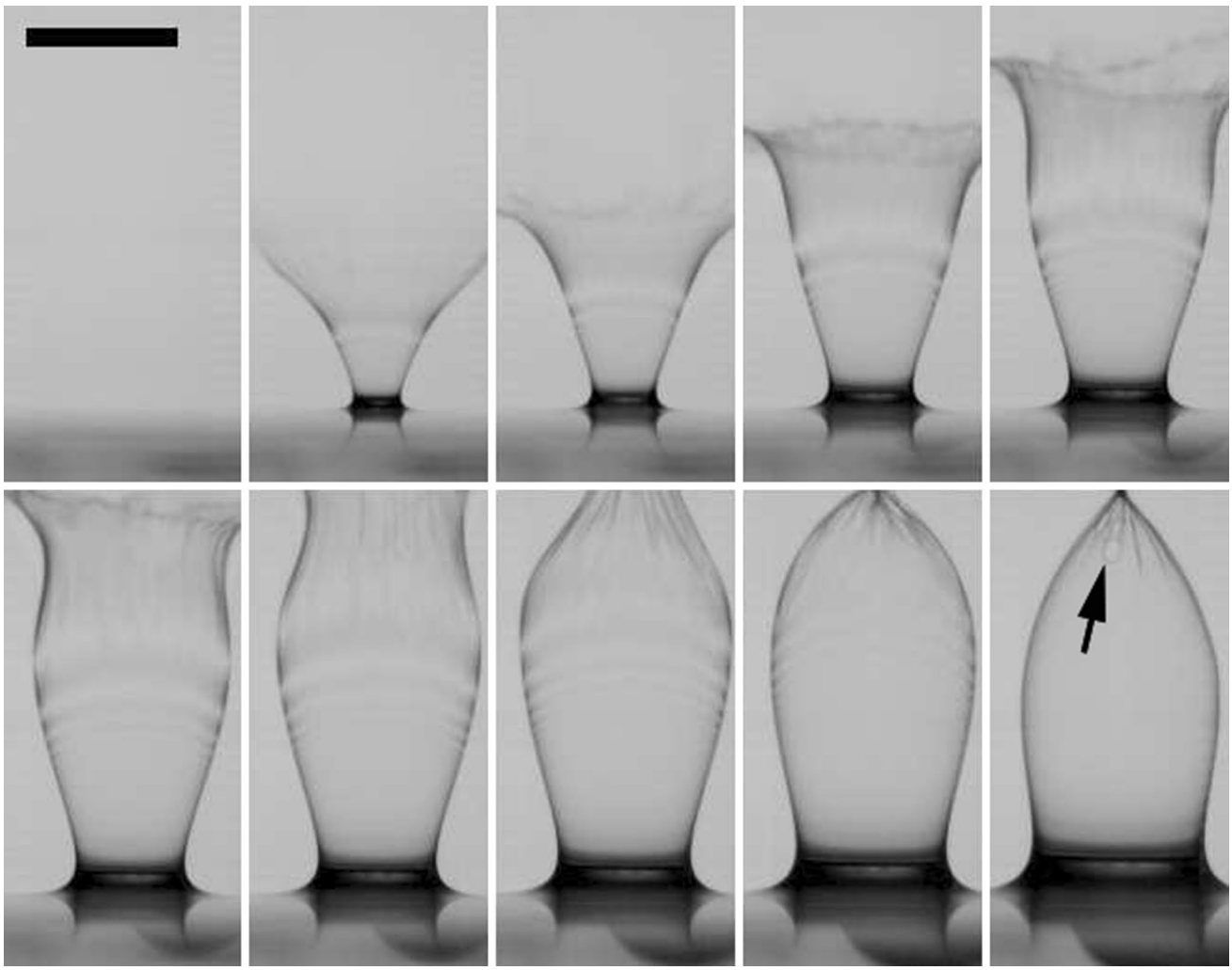

Fig. 5 Ejecta sheet evolution at reduced ambient pressure $P = 8.3$ kPa. The *arrow* in the final image indicates hole formations in the sheet as the crown seals. Images are taken at times $t = -2.9$, 2.9, 8.8, 20.6, 32.3, 44.1, 55.8, 79.4, 114.7, 173.5 μs from the laser pulse. The *scale bar* is 2 mm

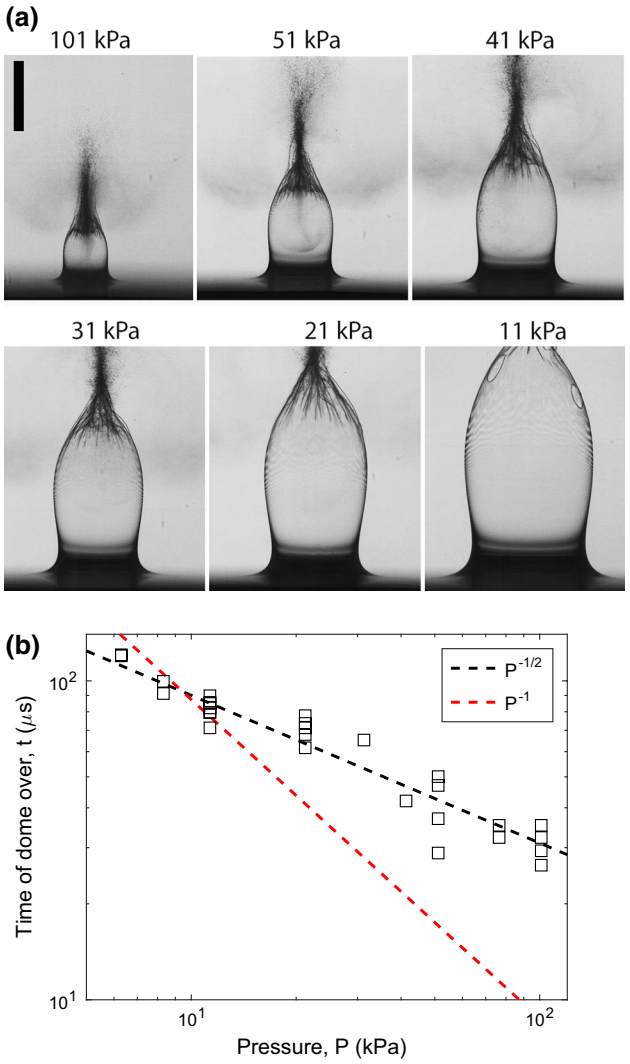

Fig. 6 **a** Images taken at the approximate time when the ejecta domes over for various pressures. The *scale bar* is 2 mm. **b** Time of ejecta dome-over versus pressure

on the order of millimeters, it is clear to see the need for ultra-high-speed photography with frame rates in excess of 1 Mfps in order to capture the dynamics. In contrast to Fig. 3, the tip of the ejecta sheet in Fig. 1 emerges at over 300 m/s based on the displacement of the tip of the ejecta over the first few frames of the video sequence. Note that this is an underestimate due to the temporal resolution used in this realization; using high temporal and spatial resolution, we find much higher ejecta speeds during the very first motion (see Sect. 3.3), which implies that the estimate of the speed from the images in Fig. 1 will have already incorporated the effects of air drag.

The ejecta sheet is initially expelled due to the rapid deposition of energy at the interface in the form of light. Specifically, focusing of the laser beam creates hotspots which result in plasma (manifested by the bright spot in the second image in Fig. 1). The plasma itself absorbs energy from the laser pulse; thus, the shape of the plasma and the size of the focal waist of the laser beam play a strong role in the shape of the ejecta. In addition, a cavity (bubble) grows rapidly below the surface (see Fig. 4 for an example sequence), providing a suction pressure pulling the ejecta walls inward, thus leading to a more streamlined shape than, for example, in water entry where the timescales of ejecta are orders of magnitude larger. Note that in Fig. 4, showing the growth of the cavitation bubble below the surface, the crown above the surface has already domed over by $t = 39\,\mu$s (image 4 in the top row), which is manifested by the hazy appearance at the edge produced by the impact of spray droplets from the crown sealing. The conical-cylindrical shape of the ejecta has been discussed previously by Apitz and Vogel (2005) and Thoroddsen et al. (2009).

3.1 Experiments at reduced ambient pressures

At reduced ambient pressure, the growth of the crown formation follows a qualitatively similar trend to that seen in water entry of spheres (see for example May 1952), whereby the dome-over phenomenon takes longer to complete. An example sequence taken at $P = 8.3$ kPa is shown in Fig. 5, where the initial crown motion is extremely rapid. We estimate the initial velocity of the tip to be $V_{\text{tip}} \approx 890$ m/s based on the displacement over the first few frames. The initial ejecta angle is similar to experiments at atmospheric pressure (e.g., Fig. 1); however, the principle difference lies in the extended growth of the crown at low pressures due to reduced air drag ($a_{\text{drag}} \propto \rho_{\text{air}}$) as compared to those at atmospheric conditions. Aristoff and Bush (2009) presented an analysis for the splash crown in water entry of spheres, citing surface tension as the primary mechanism for closure. In our case, however, the suction from the cavity below the surface is responsible for the crown sealing. The initial plasma formation leads to a sudden rise in pressure, which is the cause of the ejecta. In addition, a cavity grows below the surface (see Fig. 3). The rapid expansion of the cavity (bubble) below the surface causes a suction pressure. This competes with the high inertia in the crown and the cavity bubble growing downward, but eventually leads to closure. The fact that the closure event takes longer at reduced ambient pressures is due to the lower absolute pressure differential across the crown. Furthermore, our analysis of the sheet thickness and Weber number estimates indicates that surface tension effects are small, vindicating this argument of the closure mechanism.

The time duration from the plasma formation to the crown closure provides a timescale of the dynamics. In Fig. 6a, we present images of the crown at the approximate time of closure for a range of ambient pressures, showing a

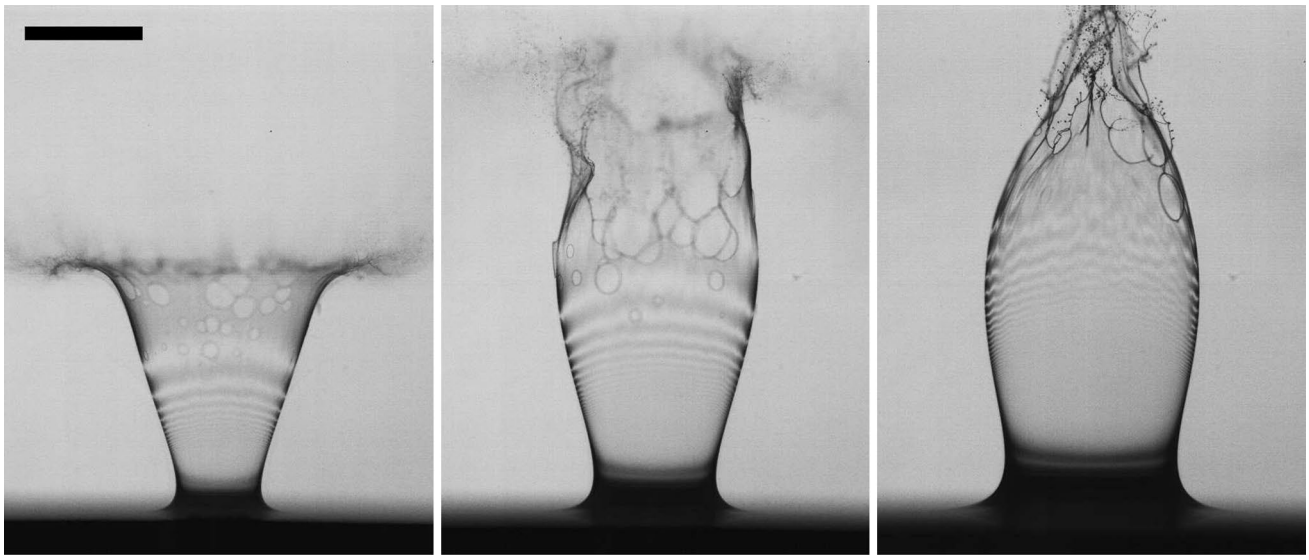

Fig. 7 Ejecta sheet evolution captured at 1 Mfps at reduced ambient pressure $P = 11$ kPa. Images are taken at times $t = 16$, 45 and 121 μs from the laser pulse. The *scale bar* is 2 mm. See also supplemental video 1

monotonic growth in the crown as the pressure is reduced from 101 kPa down to 11 kPa. We find that the time of seal scales approximately as $t \sim 1/\sqrt{P}$, as shown in Fig. 6b. This is in contrast to the established scaling laws for the surface seal time during water entry of spheres, where the quantity $\rho_a t_s V_0/D$ is constant and $t_s \sim P^{-1}$ (e.g., Lee et al. 1997; Gillbarg and Anderson 1948). As per the above arguments (see also Sect. 3.2 below), we do not expect surface tension to play a significant role in the closure; rather we attribute it to the suction pressure from the cavity below the surface leading to a pressure differential across the ejecta. The reason for the observed $1/\sqrt{P}$ dependence is, as yet, unknown.

Figure 7 presents a sequence of the crown formation at a pressure of $P = 11$ kPa, where we observe multiple ruptures in the crown wall, which appear approximately 10 μs after the laser pulse. The origins of these holes that are not presently fully understood, however, are assumed to result from a confluence of dissolved gas and film ruptures caused by van der Waals forces, a conjecture that is supported by our estimates of the film thickness (see Sect. 3.2). In particular, this sequence highlights the clarity of the interference patterns and the interaction of the light ($\lambda = 640$ nm) with the very thin crown wall. It is precisely due to the extended growth of the crown with time at reduced pressures which leads to the extended thinning and subsequent rupture (hole formation) and allows us to observe the dynamics of evolution of such thin liquid sheets which are otherwise difficult to produce in a repeatable manner.

3.2 Sheet thickness

Figure 8 shows the hole opening versus time for five particular ruptures in the ejecta sheet from the same realization shown in Fig. 7. The hole openings are clearly linear with time, indicating a constant speed, in which case the Taylor–Culick law for holes opening in a liquid film, given by $V_{tc} = \sqrt{2\sigma/(\rho\delta)}$ can be applied. The Taylor–Culick law stems from momentum conservation resulting in a simple balance between the driving force per unit length, i.e., surface tension, $F_\sigma = 2\sigma$ and the rate of change of momentum at the rim of the hole, $F_{mv} = \rho\delta V^2$. The Taylor–Culick law further assumes a constant retraction speed and film thickness preceding the rim (Savva and Bush 2009). For the data sets shown, we calculate these speeds to be 20.8, 14.8, 19.8, 11.4 and 13.7 m/s, respectively. Using these velocities, we estimate the film thickness in the crown wall as $\delta = 2\sigma/(\rho V_{tc}^2) \approx 333$, 657, 367, 1108 and 767 nm. These thicknesses, on the order of hundreds of nanometers to micrometer scales, are in excellent agreement with the ejecta sheet thicknesses found in drop impact experiments by Thoroddsen et al. (2011), where the thicknesses ranged from approximately 300 to 800 nm. At any given time, the crown wall is thinnest near the top and thickens gradually toward the base (free surface of the pool), while the entire crown gradually thickens as time progresses (see Fig. 9c).

Noting that the opening hole also travels up along the crown, we can track the hole center as a function of time, shown in Fig. 8b. The data here also exhibit a linear trend, indicating a constant speed along the crown for the duration

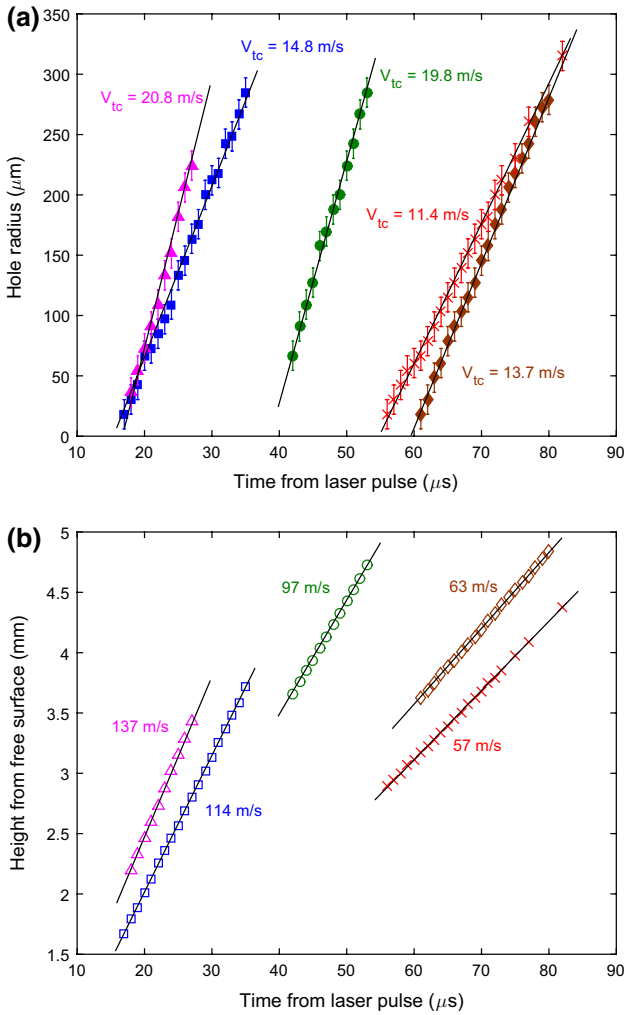

Fig. 8 **a** Hole radius versus time, measured from the laser pulse, indicating Taylor–Culick speeds. **b** Hole center distance from free surface versus time, showing translation speeds

of the hole opening, which we estimate to be $V_s = 137$, 114, 97, 63 and 57 m/s, respectively. This decrease in translation speed up the crown with time from the initial ejection is to be expected as the crown thickens and is influenced by air drag. By balancing the sheet kinetic energy, KE $\sim \rho H \delta D V_s^2$ with surface energy, SE $\sim HD\sigma$, where H and D are the ejecta height and diameter, respectively, we can construct a sheet Weber number given by

$$We_s = \frac{\rho \delta V_s^2}{\sigma} = 2\left(\frac{V_s}{V_{tc}}\right)^2.$$

Taking the sheet speeds measured in Fig. 8b, $V_s = 57-137$ m/s, we determine $We_s = 48-118$, i.e., $We = O(10-100)$, thus indicating that the ejecta, even at these small length scales, is still dominated by inertia.

The fringe patterns shown in Fig. 7 indicate that the local thickness along the crown is changing (monochromatic collimated light $\lambda = 640$ nm), due to the gradually increasing spacing between fringes (de Ruiter et al. 2015a, b). However, since the interferometry patterns have no calibration or zero reference, they alone cannot be used to directly measure the local absolute thickness. To resolve this, Fig. 9a shows that the holes translated up along the crown stay within a given fringe, which means we can use the Taylor–Culick derivation of film thickness as our inherent calibration to inform the relative interference fringe. Thus, we apply an interferometry technique to evaluate the thickness along the length of the film similar to the one employed by Choo and Kang (2001) and de Ruiter et al. (2015a, b), but instead of utilizing reflection we take advantage of transmission. Our method only works at the center of the crown where the light impinges normal to the surface of the crown based on our assumptions and following the transmission interferometry theoretical estimate. The fringe pattern is extracted from the image along a vertical line and the peaks in the pattern are matched to the theoretical peaks relative to the calibrated estimates based on the hole opening speed.

The theory thus predicts the thicknesses of the top two fringe bands identified in Fig. 9b as 787 and 1103 nm, respectively, in excellent quantitative agreement with those measured using the Taylor–Culick law. Using this inherent calibration, the correct peak from the theory is selected during the peak finding process in the image analysis, rendering plots of film thickness as a function of distance along the crown wall, shown in Fig. 9c. Keep in mind that the film thickness increases in increments of 237 nm, while the maximum deviation observed from multiple calculations of the same fringe pattern is 26 nm.

A more accurate experimental derivation of the local, time-dependent film thickness would require a more sophisticated three-wavelength, high-speed color imaging system, which is beyond the scope of this study. However, the fact that our analysis shows a very similar thickness to those found in other high-speed ejecta experiments (Thoroddsen et al. 2011; Thoraval et al. 2012) is certainly encouraging. Furthermore, our early-time data during the first 30 μs shows that the crown walls are typically less than 2.5 μm thick, and near the top, they are submicron meaning that the fine spray observed from the tip of the ejecta is comprised of droplets with submicron diameters.

3.3 Shock-wave observations

In Fig. 10, we present a snapshot from a recording taken at 5 Mfps, with effective exposure times of 20 ns. In each frame, we can clearly detect the shock wave which propagates away from the ablation site. In the very first frames

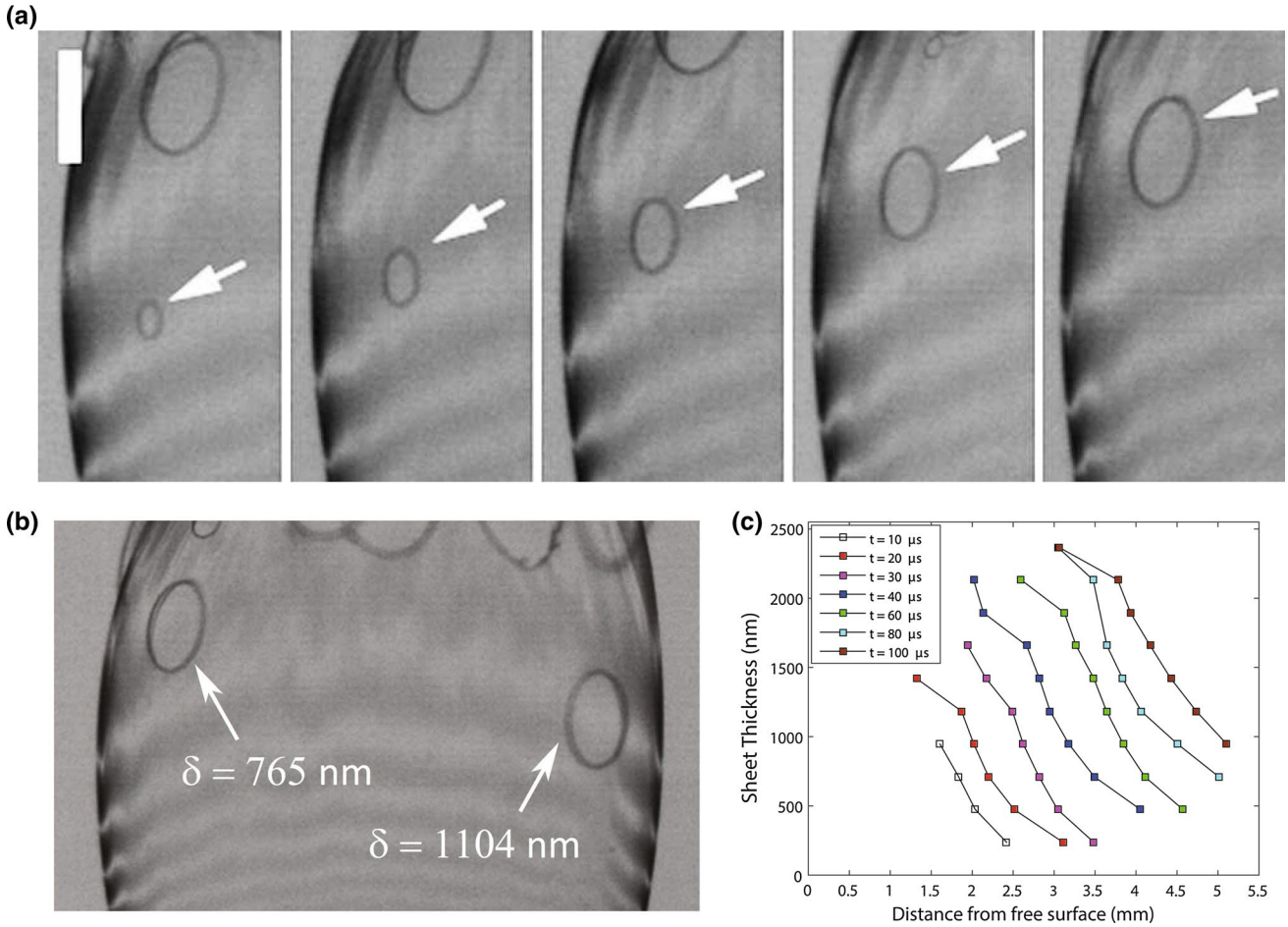

Fig. 9 **a** Image sequence showing the simultaneous growth and translation of a hole in the crown. The *arrows* indicate that the hole stays within the interference band as it moves up. The *scale bar* is 500 μm and the time between frames is 3 μs. **b** Image showing two holes in the ejecta at different heights, coinciding with two adjacent bands in the interference pattern with thicknesses measured by the Taylor–Culick law. **c** Spatially resolved film thicknesses for $t = 10-100\,\mu$s

immediately following the laser pulse, we cannot detect whether any droplets are emitted, most likely due to their sub-pixel size, which was estimated to be approximately 3 μm for water by Thoroddsen et al. (2009) and submicron from our above estimate of sheet thickness, whereas our pixel resolution is 12 μm in this case. After 1 μs, however, we can see that the ejecta tip coincides with the shock wave. As such, by measuring the location of the shock wave relative to the site of the laser focus at the free surface, we can determine the speed of the wave and thus an estimate of the ejecta tip speed. Figure 10b plots the distance of the shock wave away from the laser focal spot versus time. Noting the scales in millimeters for distance and microseconds for time, we estimate the *average* speed over the duration of the tracking to be 602 m/s, while the very early motions in the first 600 ns are much more rapid with a speed of 1.75 km/s, which yields a Mach number, $Ma = V_s/c \approx 5$.

The fit to the data over the first 5 μs, $x(t) = 1.04t^{0.49}$, indicates that the shock velocity decays as $t^{-1/2}$, i.e., $V_s \approx t^{-1/2}$. For a time of 10 μs, this would predict a velocity of just over 300 m/s, in agreement with our ejecta speed measured in Fig. 1.

The early propagation speed of the shock wave measured herein of 1.75 km/s is in good quantitative agreement with the early speed measured by Apitz and Vogel (2005) of 1.5 km/s. However, in contrast to their data, we do not observe an acceleration of the shock wave, which may be due to the temporal resolution used herein, limited to inter-frame times of 200 ns, whereas the acceleration event, described in Apitz and Vogel, occurred around 100 ns after the laser pulse. We note, however, that their laser pulse was 70 ns in duration as opposed to the 7 ns pulse used in our experiments. Finally, from the shock-wave speed, the pressure can be given by

$$P_s = \left[\frac{7}{6}\left(\frac{V_s}{c}\right)^2 - \frac{1}{6}\right] P_{\text{atm}},$$

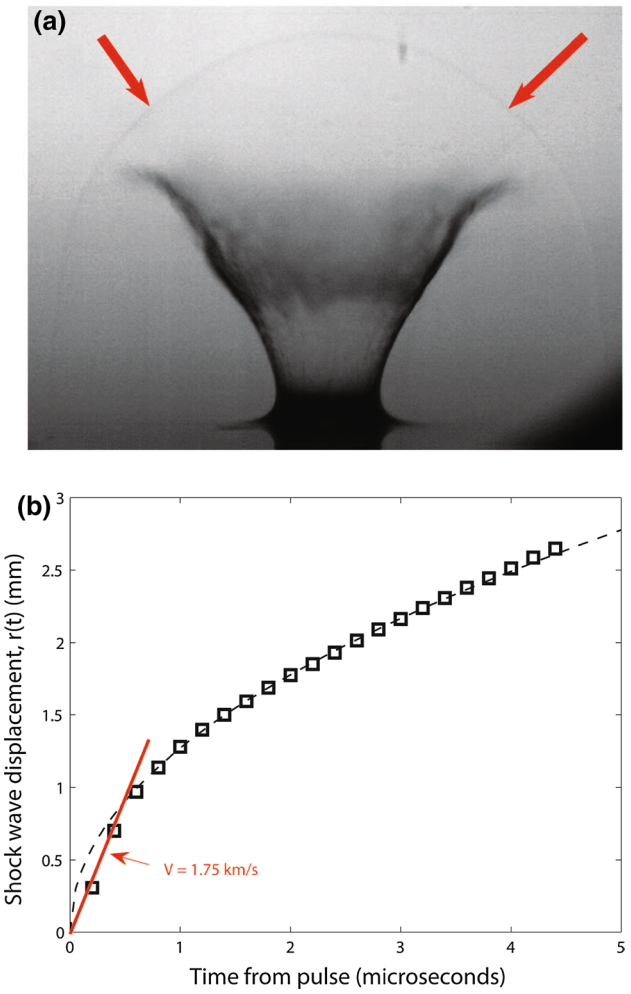

Fig. 10 **a** Image taken at $t = 1.4$ μs from a recording at 5 Mfps showing the shock wave at atmospheric pressure. The exposure time is 20 ns. The *arrows* indicate the shock wave. The *dark regions* in the *bottom corner* are due to vignetting effects of the lens. (See also supplemental video 2). **b** Shock-wave edge location as a function of time from the laser pulse. The *red line* indicates the initial speed over the first 600 ns, while the *dashed line* is a fit to the data with $x(t) = 1.04t^{0.49}$

from which we find shock-wave pressures of up to 30 atm for experiments conducted at atmospheric conditions.

4 Conclusions

We have conducted an experimental study of the effect of lowering the ambient pressure on the ablation of a flat free surface using a pulsed laser. The formation of point-plasma leads to a rapid discharge of liquid from the free surface in the form of a very fine, conical ejecta sheet. This ejecta sheet always domes over, similar to the splash sheet observed in water entry, albeit at different timescales according to the ambient pressure. As such, the motions are inertia-dominated in the very early stages and later subject to rapid pressure collapse in the cavity causing the dome-over. It was found that the sheet thickness reaches submicron length scales, as also found in ejecta sheets during drop impact onto liquid pools, while fragmentation at the tip leads to a cloud of very fine droplets, which are therefore postulated to also be submicron. The observed shock-wave motions were determined to reach speeds of up to 1.75 km/s, over five times the speed of sound in air, thus giving shock-wave pressures up to 30 atmospheres. It is hoped that the interferometric method used here can also be implemented in other phenomena exhibiting ejecta sheets to yield time-resolved thicknesses. Such efforts are presently underway.

Acknowledgments The research was partially funded by KAUST Office of Competitive Research Funds. The authors thank Jesse Belden for assistance with the interferometry calculations.

References

Apitz I, Vogel A (2005) Material ejection in nanosecond Er:YAG laser ablation of water, liver, and skin. Appl Phys A 81:329–338

Aristoff JM, Bush JWM (2009) Water entry of small hydrophobic spheres. J Fluid Mech 619:45–78

Armstrong RL (1984) Aerosol heating and vaporization by pulsed light beams. Appl Opt 23:148–155

Bird JC, de Ruiter R, Courbin L, Stone HA (2010) Daughter bubble cascades produced by folding of ruptured thin films. Nature 465:759–762

Carls JC, Brock JR (1988) Propagation of laser breakdown and detonation waves in transparent droplets. Opt Lett 13:273–275

Chen RCC, Yu YT, Su KW, Chen JF, Chen YF (2013) Exploration of water jet generated by Q-switched laser induced water breakdown with different depths beneath a flat free surface. Opt Express 21:445–453

Chitanvis SM (1986) Explosion of water droplets. Appl Opt 25:1837–1839

Choo YJ, Kang BS (2001) Parametric study on impinging-jet liquid sheet thickness distribution using an interferometric method. Exp Fluids 31:56–62

de Ruiter J, MUgele F, van den Ende D (2015) Air cushioning in droplet impact I. Dynamics of thin films studied by dual wavelength reflection interference microscopy. Phys Fluids 27:012104

de Ruiter J, MUgele F, van den Ende D (2015) Air cushioning in droplet impact II. Experimental characterization of the air film evolution. Phys Fluids 27:012105

Eickmans JH, Hsieh W-F, Chang RK (1987) Laser-induced explosion of H_2O droplets: spatially resolved spectra. Opt Lett 12:22–24

Gillbarg D, Anderson R (1948) Influence of atmospheric pressure on the phenomena accompanying the entry of spheres into water. J Appl Phys 19:127–139

Heijnen L, Quinto-Su PA, Zhao X, Ohl C-D (2009) Cavitation within a droplet. Phys Fluids 21:091102

Hsieh W-F, Zheng J-B, Wood CF, Chu BT, Chang RK (1987) Propagation velocity of laser-induced plasma inside and outside a transparent droplet. Opt Lett 12:576–578

Kafalas P, Herrmann J (1973) Dynamics and energetics of the explosive vaporization of fog droplets by a 10.6-μm laser pulse. Appl Opt 12:772–775

Lee M, Longoria RG, Wilson DE (1997) Cavity dynamics in high-speed water entry. Phys Fluids 9:540–550

Lhuissier H, Villermaux E (2012) Bursting bubble aerosols. J Fluid Mech 696:5–44

Lindinger A, Hagen J, Socaciu LD, Bernhardt TM, Woste L, Duft D, Leisner T (2004) Time-resolved explosion dynamics of H_2O droplets induced by femtosecond laser pulses. Appl Opt 43:5263

Marston JO, Thoroddsen ST (2015) 2015 Laser-induced micro-jetting from armored droplets. Exp Fluids 56:140

Marston JO, Mansoor MM, Truscott TT, Thoroddsen ST (2015) Buckling instability of crown sealing. Phys Fluids 27:091112

May A (1952) Vertical entry of missiles into water. J Appl Phys 22:1362–1372

Savva N, Bush JWM (2009) Viscous sheet retraction. J Fluid Mech 626:211–240

Tagawa Y, Oudalov N, Visser CW, Peters IR, van der Meer D, Sun C, Prosperetti A, Lohse D (2012) Highly focused supersonic micro-jets. Phys Rev X 2:031002

Thoraval M-J, Takehara K, Etoh TG, Popinet S, Ray P, Josserand C, Zaleski S, Thoroddsen ST (2012) von Karman vortex street within an impacting drop. Phys Rev Lett 108:264506

Thoroddsen ST, Takehara K, Etoh TG, Ohl C-D (2009) Spray and microjets produced by focusing a laser pulse into a hemispherical drop. Phys Fluids 21:112101

Thoroddsen ST, Thoraval M-J, Takehara K, Etoh TG (2011) Droplet splashing by a slingshot mechanism. Phys Rev Lett 106:034501

Villermaux E (2007) Fragmentation. Annu Rev Fluid Mech 39:419–446

Zhiyuan Z, Hua G, Zhenjun F, Jie X (2014) Characteristics of droplets ejected from liquid propellants ablated by laser pulses in laser plasma propulsion. Plasma Sci Technol 16:251–254